Eur. Phys. J. Special Topics **208**, 53–66 (2012)

DOI: 10.1140/epjst/e2012-01606-3

THE EUROPEAN PHYSICAL JOURNAL SPECIAL TOPICS

Regular Article

Thermal motion induced resonant forbidden reflections in wurtzite GaN

G. Beutier[1,2,a], S.P. Collins[1], G. Nisbet[1], E.N. Ovchinnikova[3], and V.E. Dmitrienko[4]

[1] Diamond Light Source, Harwell Science & Innovation Campus, OX11 0DE, UK
[2] SIMaP, CNRS - Grenoble INP - UJF, BP. 75, 38402 Saint-Martin d'Hères Cedex, France
[3] Department of Physics of Moscow State University, 119899 Moscow, Russia
[4] A.V. Shubnikov Institute of Crystallography, 119333 Moscow, Russia

Received 6 January 2012 / Received in final form 23 March 2012
Published online 15 June 2012

Abstract. We report on an experimental study of forbidden reflections in GaN (wurtzite structure) by resonant X-ray scattering at the Gallium K edge. Resonant reflections are explained by the coherent sum of a Thermal Motion Induced (TMI) scattering amplitude and a temperature independent term. We show that the shape of the TMI energy spectrum is the same for a number of reflections that are exactly forbidden by spacegroup symmetry, as well as one that relies on approximate cancellation due to special atomic sites. In addition to demonstrating new selection rules, several non-trivial aspects of the theory of TMI scattering in wurtzite crystals are quantitatively verified, including dependence on temperature, energy, azimuthal angle and polarization. The temperature-dependent and temperature independent spectra of GaN are very similar to those found in ZnO, suggesting strong similarities in the anisotropy of their electronic states. This is also supported by the strong linear dichroism observed in GaN. TMI spectra are determined by the evolution of the electronic anisotropy with nuclear position, and are likely to be extremely valuable for developing theories of electronic properties at elevated temperatures.

1 Introduction

In the early 80's, pioneering theoretical and experimental works demonstrated that resonant X-ray scattering (RXS) could excite glide-plane- and screw-axis-"forbidden" reflections [1–4]. These forbidden reflections arise because of the anisotropy of the tensor of scattering from the resonant ion, which is generally not invariant under rotation and reflection, unlike its scalar (isotropic) counterpart. While only the isotropic part is significant far from resonance, the anisotropic term is enhanced near absorption edges by multipolar electronic transitions. Nearly three decades after the first works on resonant forbidden reflections, the origin of the anisotropy of the tensor of scattering is still not fully understood, because several phenomena contribute to it [5].

[a] e-mail: guillaume.beutier@simap.grenoble-inp.fr

On top of the pure local anisotropy of the crystallographic site occupied by the resonant ions, magnetic [6], orbital [7,8] and toroidal [9] degrees of freedom can order and contribute to the forbidden reflections. The case of magnetic order probed by RXS is well understood because it can be described within the familiar electric dipole approximation, and is closely related to other techniques such as neutron diffraction. Orbital and toroidal ordering, on the other hand, are often more complex and contentious (see, for example, a recent report on magnetite which concluded that charge and orbital ordering play a relatively minor role in the diffraction signals compared to a small lattice distortion [10]).

Forbidden reflections become weakly allowed when atoms are displaced from positions of high symmetry. If the time-averaged atomic displacements are coordinated in a way that conserve the crystal symmetry, the "forbidden" reflections will be observed at a resonance only. Such atomic displacements can be due to static disorder (like chemical impurities) or dynamical disorder [11]. So-called Thermal Motion Induced (TMI) scattering belongs to the latter case and is a manifestation of the activation of optical phonons. Despite having been predicted more than ten years ago [12], it has so far been reported in only two materials: in Germanium [13,14] and in the wurtzite form of zinc oxide (ZnO) [15]. In both systems, the measured forbidden reflections result from the interference of two contributions, one temperature independent and one temperature dependent. The latter, attributed to TMI scattering, is thought to be related to the mean square of the atomic displacements. The origin of these two contributions is still not settled, due to a sparsity of experimental data and appropriate theory. It is suggested that electric dipole-quadrupole scattering events dominate the temperature independent part and that the dipole-dipole events, forbidden at the rest position, contribute to the temperature dependent part via its derivatives with respect to the positions of the resonant atoms and of their neighbours [16,17]. In Germanium, the 006 forbidden reflection energy lineshape shows little change with the temperature [14], suggesting that the temperature dependent and temperature independent contributions have similar spectra and therefore possibly the same origin, while in ZnO the 115 forbidden reflection line shape shows strong variations, pointing at two very different spectra [15]. It is clear that the physics of the material itself lies within these two spectra, whatever their origin, and that several systems must be compared in order to understand better which physical phenomena are involved in TMI scattering and what relevant information the technique will yield.

In this paper, we report TMI scattering in the wurtzite form of Gallium Nitride (GaN) at the Gallium K edge. We demonstrate the universal nature of the TMI-scattering spectrum in GaN by measuring several forbidden reflections. In particular, we show that reflections forbidden only by the specific rules of the crystallographic site of the resonant atoms have the same TMI-scattering spectrum as the reflections forbidden by the general extinction rules of the space group. They also have the same temperature-independent spectrum, except for a small non-resonant part contributing to the space-group allowed reflections, due to aspherical electron density and/or anharmonic motion. We also performed a full quantitative verification of theoretical predictions about the TMI-scattering cross-section: The azimuthal and polarization dependences are in good agreement with the theory, and the cross-section of hhl reflections varies as h^2 and is independent of l.

Moreover, we compare the present results with those obtained previously on the similar compound ZnO. The wurtzite forms of GaN and ZnO have very similar structures and constitutive ions [18,19], and thus very similar electronic structures [35]. We find that their temperature independent and temperature dependent spectra contributing to forbidden reflections are very similar.

Additionally, we retrieved the absorption cross-section of GaN from fluorescence measurements and we observed a strong linear dichroism, again very similar to ZnO.

2 Theoretical

The wurtzite structure is depicted in Fig. 1 of [17]. It belongs to the crystallographic space group $P6_3mc$, No. 186. All atoms in the structure occupy special crystallographic sites labelled $2b$ [20], with point symmetry $3m$. Pairs of atoms on $2b$ sites are related by a 2_1 screw axis along the c-axis. The crystal has therefore two types of forbidden reflections: those of the type, hhl with l odd, which are forbidden by the general rules of the space group, and those of the type hkl with l odd and $h-k=3n$, which are forbidden by the special rules of the sites $2b$. It is straightforward to show that the unit cell structure factor of the tensor of scattering is written the same way for both types of forbidden reflections:

$$F\left(hkl\right) = f - R_{\pi}^{c}\left(f\right) \tag{1}$$

where f is the atomic tensor of scattering of a resonant atom of the unit cell, and R_{π}^{c} the rotation operator associated to the 2_1 screw axis along the c-axis. Because of the $3m$ symmetry of the $2b$ sites, the rank 2 tensors are uniaxial along the c-axis and cancel out in the structure factor of the forbidden reflections. Thus only tensors of at least rank 3 can contribute to the forbidden reflections. Moreover, rank 3 symmetric tensors compatible with the $3m$ symmetry have at most 4 independent components [21] and all but one cancels out in Eq. (1). In a (x, y, z) Cartesian basis with x, y and z axes parallel respectively to the crystal mirror-plane, glide-plane, and 6-fold axis [22], the single surviving independent component of any rank 3 tensor f in Eq. (1) is $f_{xyy} = f_{yxy} = f_{yyx} = -f_{xxx}$. The next step is to identify the scattering processes described by rank 3 tensors.

RXS is usually described in terms of electronic multipolar resonances, strongly dominated by electric dipole and electric quadrupole interactions. Pure dipole-dipole (E1E1), pure quadrupole-quadrupole (E2E2) and mixed dipole-quadrupole (E1E2) terms can interplay in RXS, leading to complex azimuthal and energy dependences of forbidden reflections, particularly if the resonant ions occupy different crystallographic sites [23]. The E1E1 contribution is normally the strongest, but it is described by a rank 2 tensor and thus cancels out in the structure factor of forbidden reflections in wurtzite crystals. This allows for easier observation of weaker processes such as higher order electric multipoles and TMI scattering. An important property of the sites $2b$ is that they are not centro-symmetric, allowing for parity-odd tensors, such as the rank 3 E1E2 tensor. This has allowed unusual optical activity to be observed in diffraction from these crystals [24]. The symmetry also allows for a single component of the rank 4 E2E2 tensor [25], but we shall ignore it in the following because it is expected to be much weaker than the E1E2 tensor, based on numerical simulations with the code FDMNES [26], and we find no experimental evidence for such a term.

Although the E1E1 tensor does not contribute to forbidden reflections in the time-averaged structure of an ideal wurtzite crystal, thermal vibrations distort the symmetrical environment of the resonant atoms, enabling a non-vanishing average of E1E1 scattering: this is TMI scattering. It is modelled by a rank 3 tensor built with the derivatives of the rank 2 E1E1 tensor with respect to the atomic displacements. It couples to the diffraction vector $\mathbf{Q}$ and to the polarizations $\boldsymbol{\epsilon}$ and $\boldsymbol{\epsilon}'$ of the respectively incident and scattered beams [11]. Like the E1E1 scattering tensor from which it is derived, it is symmetrical with respect to the polarization indices. These last two properties are also true for parity-odd time-even (non-magnetic) rank 3 tensors [27] such as the E1E2 contribution in the present case.

Compiling the above listed properties and after contracting the third rank tensors with the scattering vector, one obtains a simple expression for the scattering cross-section:

$$\left|F\left(hkl,\psi,E,T\right)\right|^2 = \left|f_{E1E2}(E) + f_{TMI}(E,T)\right|^2 \times \left|\boldsymbol{\epsilon}(hkl,\psi)\boldsymbol{A}(hkl)\boldsymbol{\epsilon}'(hkl,\psi)\right|^2 \tag{2}$$

with

$$\boldsymbol{A}(hkl) = \frac{1}{2}\begin{pmatrix} k-h & (h+k)\sqrt{3} & 0 \\ (h+k)\sqrt{3} & h-k & 0 \\ 0 & 0 & 0 \end{pmatrix} \tag{3}$$

where E is the energy of the X-rays, T the temperature of the sample and ψ the azimuthal angle. f_{E1E2} and f_{TMI} are complex scalar functions describing respectively the E1E2 and TMI scattering amplitudes. The azimuthal and polarization dependences of the intensity are entirely determined by contracting the polarization vectors with the matrix $\boldsymbol{A}(hkl)$. The relative strength of different forbidden reflections is also determined by this matrix. It is independent of l. Note that for $h = k$ it reduces to the simpler form used in [15,17,28], and the cross-section becomes proportional to h^2.

We note that Eq. (2) shows no difference between space group forbidden and special site forbidden reflections. In particular, TMI-scattering is involved with the same amplitude and therefore it is expected that both types of forbidden reflections have the same fundamental spectrum and the same temperature-dependence. An experimental verification of this prediction [11] is one of the objectives of the present study. A fundamental difference between the space-group forbidden and the special site forbidden reflections is that the latter allow for an additional non-resonant contribution due to (1) the asphericity of valence electronic density and (2) the anharmonicity of thermal vibrations, which is particularly strong in Wurtzite crystals [29]. This non-resonant amplitude will interfere with the resonant amplitude, allowing interesting interference effects. The effect of anharmonicity is known to be strongly temperature-dependent and to be related to the change of the c lattice parameter [29]. Moreover its temperature-dependence is expected to be different from that of TMI-scattering, which is dominated by harmonic vibrations.

It is clear from Eq. (2) that E1E2 and TMI scattering cannot be distinguished by looking at different forbidden reflections, different azimuths or different polarization channels, since these factors are common to both processes. As stated in [15] for the particular case of hhl forbidden reflections, they can be disentangled only due to their different energy spectra and the change of their interplay with temperature. Indeed, E1E2 scattering is almost temperature-independent (except for the weak thermal dependence of the average structure [17]), while TMI scattering is strongly temperature-dependent because it is generated by thermal vibrations. To first approximation, TMI scattering is dominated by harmonic vibrations and more precisely optical phonons. Acoustic phonons with small wave-vectors do not contribute because these modes move each unit cell as a whole and no anisotropy appears [11]. Not all optical modes contribute to TMI-scattering either, because some of them respect the site symmetry of the resonant atoms: in the case of wurtzite crystals, the two optical modes along the c-axis do not enable resonant scattering [17]. Since the population of phonon density of states follows Bose-Einstein statistics, an empirical law was proposed to explain the temperature dependence of the TMI scattering amplitude [14,15], allowing the spectral part of Eq. (2) to be written as follows:

$$|f_{E1E2}(E) + f_{TMI}(E,T)|^2 = \left|A(E) + B(E)\coth\left(\frac{\hbar\omega_0}{2k_BT}\right)e^{-i\Phi(E)}\right|^2 e^{-2M} \tag{4}$$

with $A(E) = |f_{E1E2}(E)|$, $B(E)$ the modulus of the fundamental spectrum of f_{TMI}, and their relative phase $\Phi(E)$. Acoustic phonons are taken into account by the Debye-Waller factor e^{-2M}. This approach considers only optical phonons at the Γ point, taken to have an effective energy $\hbar\omega_0$. Their population is given by the hyperbolic cotangent term. To go beyond this approximation, it is also possible to decompose

TMI scattering in different contributions including the autocorrelation of the displacements of the resonant atoms and the cross-correlations of the displacements of the resonant atoms and surrounding atoms. This is discussed in details in [17] but such analysis is not the purpose of the present paper.

3 Experimental results

Forbidden reflections of GaN were measured around the Gallium K edge (∼10.367 keV) as a function of hkl, energy, azimuth and temperature. We measured the following forbidden reflections: 115, 117, 225 and 303. For the 115 and 225, two equivalent reflections were measured (for instance $\bar{1}25$ and $\bar{2}15$ for the 115); for the 117, three equivalent reflections were measured. The 115, 225 and 117 reflections are forbidden by the general rules of the space group, while the 303 is forbidden by the specific rules of the 2b crystallographic site.

Measurements were performed at beamlines XMaS at the ESRF and I16 at Diamond Light Source. At both beamlines the synchrotron beam was monochromatized with a Si 111 double bounce monochromator. The natural horizontal polarization delivered by the bending magnet (XMaS) or undulator (I16) was utilized. Most measurements presented here were made without polarization analysis, but in a few cases, the polarization of the scattered beam was analyzed with the 008 reflection of a graphite crystal. Diffraction was measured in the vertical plane, using a silicon drift detector for energy resolution, allowing the separate but simultaneous recording of the elastic scattering and the fluorescence yield. The sample was a large (several tens of mm^2) single crystal with the c axis normal to the surface, purchased from Lumilog and mechano-chemically polished by Novasic. The sample was mounted on the diffractometer in a closed-cycle cryo-furnace and the temperature range covered 35 K–800 K. Another furnace was used for additional higher temperature measurements, up to 1000 K.

Allowed reflections were strong ($\approx 4 \times 10^{10}$ counts per second from the 002) and their rocking-curve full width at half maximum (FWHM) about 0.1°. Forbidden reflections were as strong as several 10^4 counts per second above the background in favourable cases. Their rocking curves were almost Gaussian in shape, with FWHM varying between 0.08° and 2°, depending on the reflection and the azimuth and independently of the temperature.

In order to verify the symmetry analysis developed above, we measured the azimuthal dependence of the 115 reflection with and without polarization analyser (Fig. 1). Only part of the azimuthal range could be covered, due to the large angle (33°) between the 115 reflection and the surface normal (001). The azimuth $\psi = 0$ is such that the $\langle 001 \rangle$ direction is in the scattering plane, pointing on the side of the scattered beam. The azimuthal dependence was found in good agreement with the predictions of Eq. (2). It is notably independent of the energy and the temperature. We could therefore carry the spectral measurements at a single azimuth, and simply correct the intensity for the azimuthal dependence. Azimuthal positions far enough (>1°) from multiple scattering contaminations were chosen to record the spectra of the reflections: $\psi = 0$ for the 117 and 225, $\psi = -24°$ for the 115, and $\psi = 90°$ for the 303.

In the following, in order to compare quantitatively the recorded spectra, they were systematically corrected for the following effects:

- The variation of mosaicity was taken into account by measuring rocking curves at fixed energy: the spectra, were corrected by the ratio of integrated intensity to peak intensity. The Lorentz factor is included in the rocking curve integration.

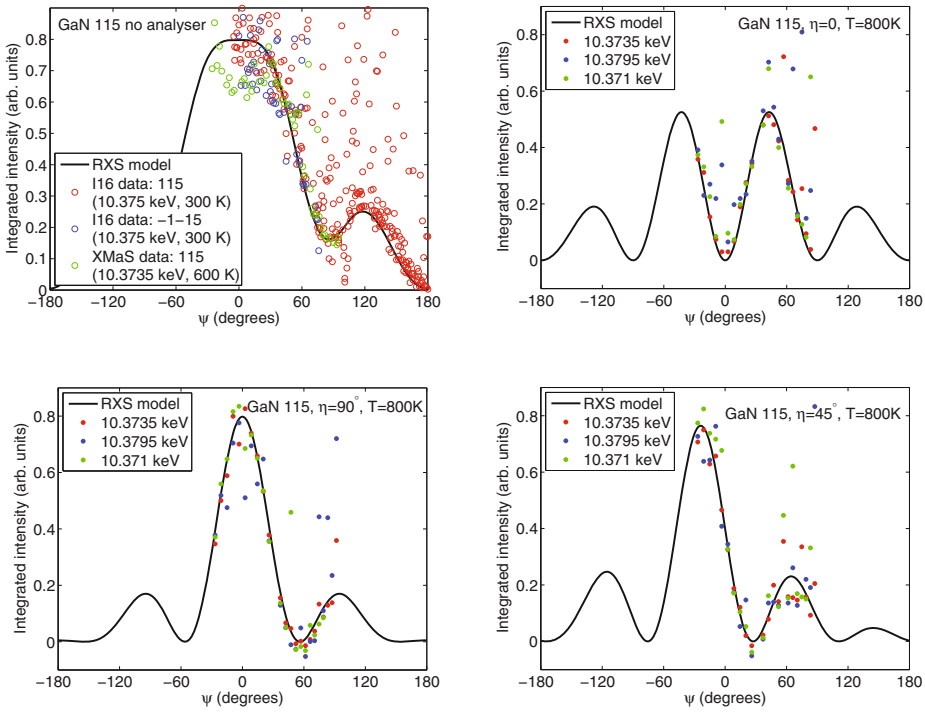

Fig. 1. Azimuthal dependence of the 115 reflection. The azimuth is zero when the $\langle 001 \rangle$ direction is in the scattering plane, pointing towards the scattered beam. Measurements were done on both beamlines, at various energies and temperatures, with and without analysing the polarization of the scattered beam. The self-absorption effect, which also depends on azimuth, was taken into account for the calculated data. The deviation from the model is attributed to multiple scattering, appearing as random noise. Its high density, due to the small lattice parameters and the small wavelength, is in agreement with calculations (not shown here). Note that the multiple scattering contamination is mostly positive, but occasionally negative due to destructive interference. Upper left panel: no polarization analyzer. Other three panels: linear polarization rotated by an angle η with respect to the direction of polarization of the incident beam. Upper right: $\eta = 0$ (σ polarization). Lower left: $\eta = 45°$. Lower right: $\eta = 90°$ (π polarization).

– The resonance spectra were corrected for self-absorption using an isotropic absorption spectrum obtained by measuring the transmission of powder from the same sample. This crude correction induces distortions of the spectra, because strong linear dichroism is observed in GaN (see Appendix), as in ZnO [24]. However, this allows for an easy correction and better comparison with RXS spectra measured in ZnO, which were also corrected with an anisotropic absorption spectrum. In this approximation of isotropic absorption, the measured RXS intensity $I(E)$ is [30]:

$$I(E) \propto \frac{|F(E)|^2}{\mu(E) \times (1+g)} \tag{5}$$

where $g(\psi)$ is a geometrical coefficient that depends (among others) on the azimuth ψ. Therefore, the spectra were corrected with the absorption spectrum according to $|F(E)|^2 \propto (1+g)\mu(E)I(E)$.

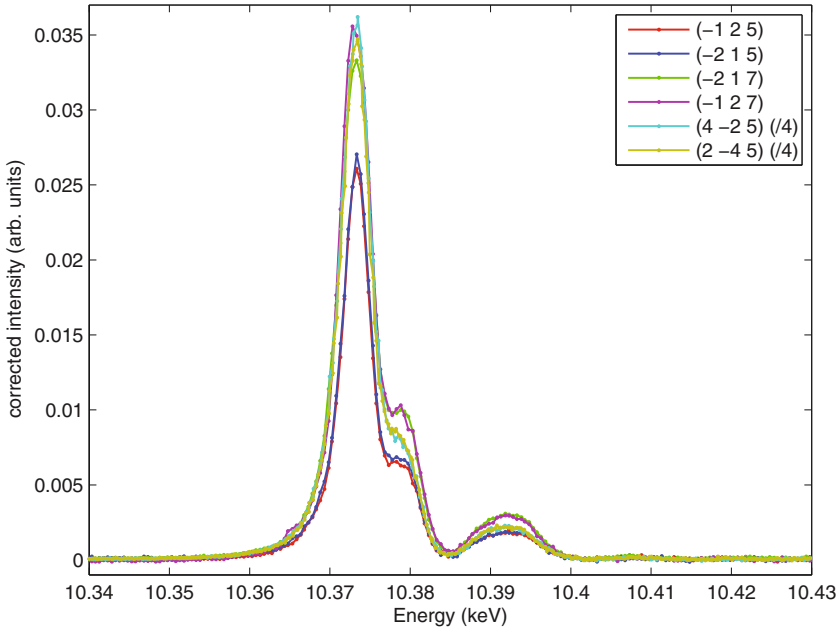

Fig. 2. Corrected intensity spectra of several forbidden reflections of the type hhl (divided by h^2): $\bar{1}25$ and $\bar{2}15$ are equivalent to 115; $\bar{1}27$ and $\bar{2}17$ are equivalent to 117; $4\bar{2}5$ and $2\bar{4}5$ are equivalent to 225. The spectra are almost identical by equivalent pairs, giving confidence in the quality of the data and the data correction procedure. All reflections were measured between 900 K and 1000 K, temperatures at which TMI scattering is largely dominant.

– The spectra were normalized by the polarization dependence calculated from Eqs. (2) and (3), and by the Debye-Waller factor e^{-2M}, calculated with the formalism given in [32].

4 Discussion

The corrected intensity spectra of several reflections of the type hhl, measured between 900 K and 1000 K, are presented in Fig. 2. In this temperature range, the intensity is largely dominated by TMI scattering. The similarity of the spectra is in good agreement with the prediction of a unique TMI scattering spectrum. The main difference in lineshape appears around 10.379 keV between the 225-type reflections and the others. We ascribe it to the linear dichroism in the self-absorption effect, which is maximum at this energy (Fig. 6). The relative intensities of the spectra are almost proportional to h^2 and independent of l, as predicted in Eq. (2). The intensity of 115-type reflections appears nevertheless lower than expected. The relative intensities of the spectra are very sensitive to the Debye-Waller factor, evaluated using the parameters for Ga ions in GaN calculated in [32] and found in good agreement with recent experimental work [33]. There is however a wide range of values reported in the literature, with equivalent Debye temperature ranging from 365 K to 657 K [34]. Using alternative vibrational parameters for the Debye-Waller evaluation can modify the relative intensities enough to make the 115-type reflections match the prediction.

The spectra of the 115 and 303 reflections were measured as a function of temperature between 37 K and 801 K (Fig. 3). The corrected intensity maps were fitted to Eq. (4) with $\hbar\omega_0 \sim 18$ meV [31]. As in the case of ZnO [15], the exact value of

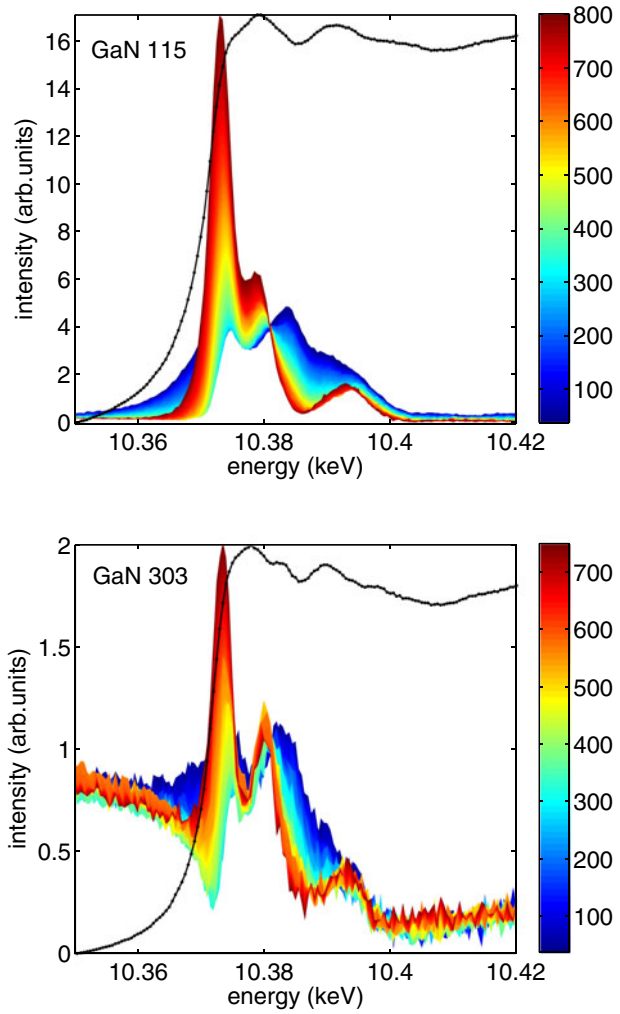

Fig. 3. Temperature dependence of the energy spectra (not corrected for self-absorption) of the 115 (top) and 303 (bottom) reflections. The color scheme indicates the temperature. Typical fluorescence spectra, found independent from the temperature, are also shown in black.

$\hbar\omega_0$ was found to have little influence on the quality of the fit. The results of the fits are shown in Fig. 4, together with those found for ZnO. There is a striking similarity between the three considered reflections, i.e. 115 in GaN, 303 in GaN and 115 and ZnO, in their fundamental spectra $A(E)$ and $B(E)$ and their phase difference $\Phi(E)$. In all three cases, the main resonances of $A(E)$ are packed together in a broad and structured peak, while the main resonances of $B(E)$ are separated in two sets. A phase jump of π that could be guessed in ZnO appears clearly in GaN for both reflections. Since $B(E)$ vanishes at the same point, it suggests that its real amplitude changes sign.

First we shall discuss the spectra retrieved for GaN. Despite the (not unexpected) similarity between the spectra retrieved from the 115 and 303 reflections, some differences can be seen. Offsets have been fitted in order to match the spectra $A(E)$ and $B(E)$ of the 303 reflection with those of the 115 reflection: we find a strong offset

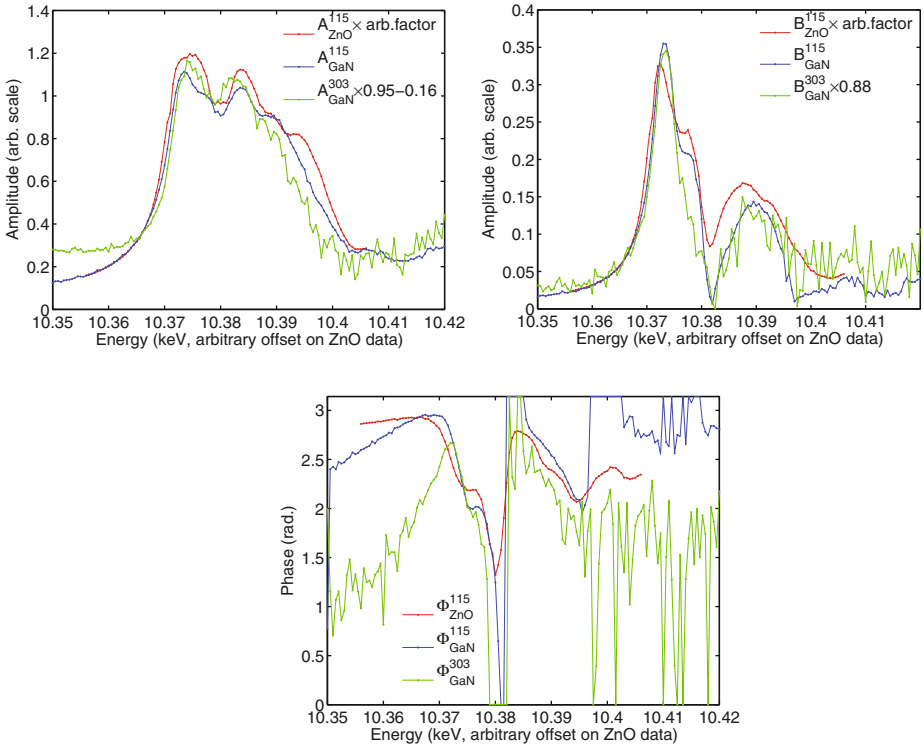

Fig. 4. Results of the fits against Eq. (4) of the 115 and 303 forbidden reflections intensity in GaN and of the 115 forbidden reflection intensity in ZnO. Top left: temperature independent contribution ($A(E)$). Top right: temperature dependent contribution ($B(E)$). The same scaling factor was applied to the values of $A(E)$ and $B(E)$ for ZnO. The values of $A(E)$ and $B(E)$ found for the 303 reflection of GaN were linearly fitted to those found for the 115 reflection of GaN. As expected, the linear coefficient is the same for both curves, while the offset is non-zero only for $A(E)$: it is due to non-resonant scattering. Bottom: Relative phase $\Phi(E)$ (in radians) between $A(E)$ and $B(E)$. The same energy offset was applied to the ZnO data in all graphs. ZnO data taken from [15]. The isotropic absorption obtained by powder transmission measurements was used to correct the data of GaN from self-absorption, as had been done for ZnO.

of the temperature independent spectrum $A(E)$, due to the non-resonant scattering, which is mostly temperature and energy independent. It is also clearly evidenced in Fig. 3, where the intensity of the 303 reflection does not vanish off-resonance, unlike the 115 reflection. Conversely, the offset of the temperature dependent spectrum $B(E)$ is not significant compared to the noise level. It shows that there is no significant non-resonant contribution with the particular temperature behaviour described in Eq. (4). Non-resonant scattering occurs at reflections forbidden by the special site symmetry because of the aspherical electronic density and/or anharmonic thermal vibrations, which are strong in wurtzite crystals [29]. Although anharmonic thermal vibrations can depend on temperature, there is no simple model to describe their temperature dependence in GaN. The small number of temperature values measured at the 303 reflection was insufficient to determine any significant deviation of the experimental data from our model. Except for the non-resonant scattering, the spectra $A(E)$ retrieved from the 115 and the 303 reflections are very similar, consistent with our model which has the same unique component of the E1E2 tensor for all forbidden

reflections. But some slight differences remain which are significant above the level of background noise. Possible explanations for these differences are the linear dichroism of the absorption spectrum, which has been ignored for the self-absorption correction, and interference between resonant and non-resonant amplitudes. Similarly, the temperature dependent spectra $B(E)$ retrieved from the 115 and 303 reflections are almost identical, except for a missing resonance around 10.378 keV for the 303 reflection. To first approximation, the resemblance confirms the prediction that TMI scattering has the same spectrum for both types of reflections.

Now we shall compare the spectra retrieved for GaN and ZnO. The spectra derived from their 115 reflections are very similar. Such similarities between the two materials are not surprizing: they have almost identical crystal structures, with only slightly different lattice parameters and apical lengths of the tetrahedra, and their constituent atoms are neighbours in the periodical table of elements. RXS is a spectroscopy of the excited state of the electrons in the resonant ions. Although the electronic structures of the excited states in these materials are not known, numerous studies of the electronic structure of the ground state in wurtzite crystals are available in the literature (see references in [35]). They show that GaN and ZnO have very similar electronic band structures in the ground state. One can infer that the excited states also have similar electronic structures. In particular, Xu & Ching [35] show a direct comparison of the band structures, densities of states and dielectric functions for GaN and ZnO. It is therefore not surprizing to observe similar RXS spectra for these crystals. In the case of the temperature independent spectrum, which we associate with E1E2 resonances, it is closely related to the electronic structure of the material. In the case of the temperature dependent spectrum, which we associate with TMI scattering, the relation with the electronic structure is less direct, because E1E1 resonances contribute through their derivative with respect to atomic positions, i.e. we probe the evolution of the electronic structure with nuclear positions. Simulations performed with the code FDMNES [26] confirm that GaN and ZnO have very similar atomic scattering tensor components. The single E1E2 component contributing to the 115 reflection, and the single E1E1 component whose derivative is responsible for the TMI are shown in Fig. 5. From the above considerations, we build confidence that the spectra extracted from the fit procedure are reliable. Looking beyond the similarities in their general shape, the spectra of the two materials also show small but clear differences. Understanding these differences will provide a challenge for electronic structure calculations.

5 Conclusions

We have studied forbidden reflections in wurtzite GaN. The proposed model of resonant X-ray scattering in wurtzite crystals is confirmed in many important aspects (azimuth-polarization dependence, relative strength of the reflections). In particular, the measurements support the existence of two, and only two, fundamental spectra of the material participating to all forbidden reflections, independently of the Miller indices, even for reflections that are not forbidden by the space group rules but only by the special site symmetry. The first is temperature independent and of E1E2 origin. The second one is temperature dependant and in good agreement with the Bose-Einstein statistics of optical phonons. These two fundamental spectra, as well as the strong linear dichroism evidenced in the absorption spectrum, are very similar to those found in another wurtzite material, ZnO. However, small differences have been highlighted, thus demonstrating the sensitivity of the technique to small variations in excited electronic states. Further measurements on other materials, for instance on other wurtzite compounds with less similar constitutive elements, are

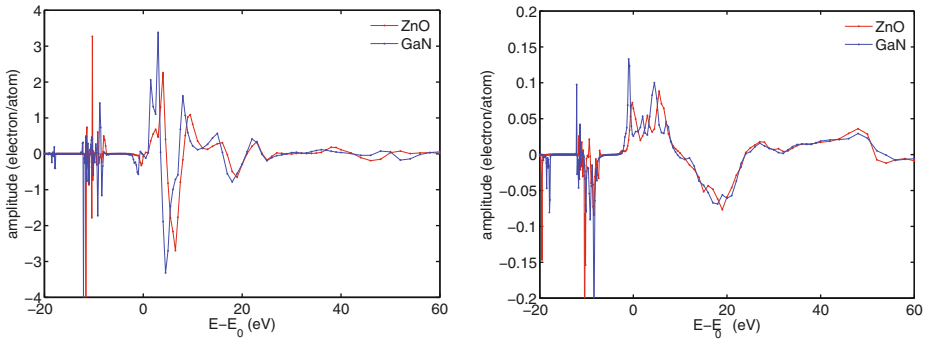

Fig. 5. FDMNES simulation of the atomic scattering tensor of the resonant atom in its high symmetry site in ZnO and GaN. Left: single non-zero E1E1 component; its structure factor vanishes at forbidden reflections, but its derivative with respect to the atomic position participates to the TMI. Right: single non-vanishing E1E2 component in the structure factor of forbidden reflections. Energies are given relatively to the resonance edge. The sharp features more than 5 eV below the resonance are below the Fermi level and are not measured in RXS. Calculations were performed using a muffin-tin potential, and no convolution has been applied (see [26] for details).

needed to better understand the origin of the differences and similarities. The results of these and future measurements should provide a valuable and unique test of theories that address the *change* in electronic ground-state with atomic position driven by optical phonons, essential for understanding the electronic properties of materials at elevated temperatures. Moreover, this study shows that particular care should be given to the temperature dependence when measuring forbidden reflection with no E1E1 contribution: the intensity and the spectrum can be severely altered by the thermal motion induced scattering. The effect is nevertheless absent in several compounds [40], with no obvious reason. We believe that *ab initio* calculations will lead to a better understanding of the relevant parameters involved in thermal motion induced scattering.

The authors acknowledge the support of the XMaS staff for the RXS measurements at ESRF.

6 Appendix: Linear dichroism in GaN

In our data treatment, we corrected the intensities for self-absorption, based on an absorption spectrum determined by measuring the transmission through a powder sample of the same crystal (Fig. 7). This method yields an orientationally averaged absorption spectrum. However GaN actually exhibits strong linear dichroism, like ZnO [24].

In order to characterize the dichroism, we measured fluorescence spectra of the sample for various incidence angles, various azimuthal angles with respect to the six-fold axis, and two perpendicular linear polarizations of the incident beam (Fig. 6). As expected for point group 6*mm*, no azimuthal dependence was found with respect to the six-fold axis. As the quadrupolar features are expected to be more than order of magnitude weaker than the dipole contribution, we treat the absorption cross-section in the dipole approximation, in which the point group 6*mm* is dichroic [36]. Although the linear polarization vector is generally not an eigenstate of the optical system, we can make this approximation if the anisotropy is not too strong compared to the

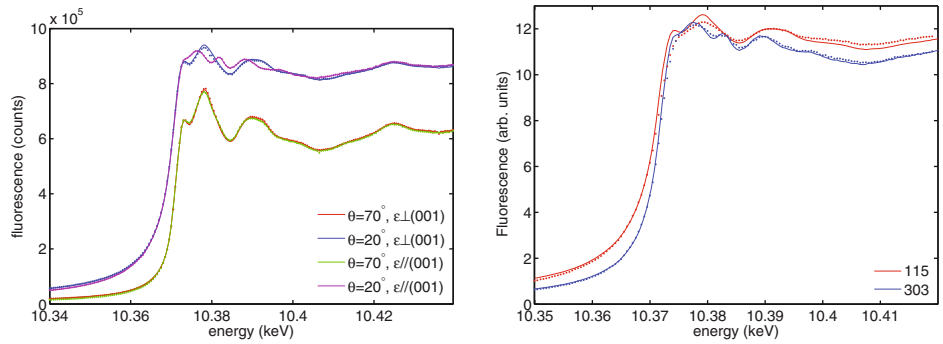

Fig. 6. Left: Fluorescence measurements (dots) and fits (lines) on GaN around the Ga K-edge. The measurements were carried out on Beamline I16 with polarization horizontal and the detector directly above the sample, and in the horizontal plane of the sample, for two incident angles (20° and 70°). The fundamental absorption spectra were obtained from these four measurements only. The excellent quality of the fits mean that they are indistinguishable from the data. Right: fluorescence curves (dots) recorded during the measurement of the 115 and 303 reflections at the XMaS beamline, together with the corresponding spectra calculated from the fundamental spectra obtained at I16 (lines). A shift of 1 eV between the energy calibration of the two beamlines was applied to better match the data.

isotropic absorption. Within this approximation, the linear absorption coefficient μ characterizes the intensity exponential decay with no change in polarization. According to Brouder's formalism [36], μ can be written in the dipole approximation as:

$$\mu(E,\theta) = \mu_{nres} + \mu_K(E,\theta) = \mu_{nres} + \mu_0(E) - \frac{1}{\sqrt{2}}\left(3\cos^2\theta - 1\right)\delta\mu(E) \qquad (6)$$

where the non-resonant part of the absorption μ_{nres} is almost constant across the K-edge, whereas the resonant part at the K-edge, μ_K, is different for different linear polarization states. μ_0 and $\delta\mu$ are respectively the isotropic and anisotropic parts of μ_K. The absorption cross-section depends only on the angle θ between the polarization vector and the c axis.

For a thick sample, the measured fluorescence intensity I_f normalized by the incident flux I_0 is [37]:

$$\frac{I_f(E)}{I_0(E)} \propto \frac{\mu_K(E)}{\mu(E) + g\mu(E_f)} \qquad (7)$$

where the angular dependence is implicit. g is a known geometrical coefficient dependent on the incidence and exit angles, and therefore on θ. $E_f = 9.569\,\text{keV}$ is the average energy of the K fluorescence lines, weighted with their relative intensities [38]. The fluorescence spectra were fitted against Eqs. (6) and (7) with $\mu_0(E)$, $\delta\mu(E)$ and a scale factor as free parameters. The resulting isotropic and anisotropic spectra are shown in Fig. 7. The measured and fitted fluorescence lines do not show any difference, attesting for the excellent quality of the fit (Fig. 6). The anisotropic part of the absorption is clearly evidenced and is about one order of magnitude lower than the isotropic part.

The results are well reproduced with XANES calculations performed with the code FDMNES [26], using a simple muffin-tin potential. Note that there is no scaling parameter. From the two spectra obtained by the fluorescence measurements, we can calculate the absorption and fluorescence for any geometry. The strongest dichroic effect is obtained between $\theta = 0$ and $\theta = 90°$. The fluorescence spectra calculated

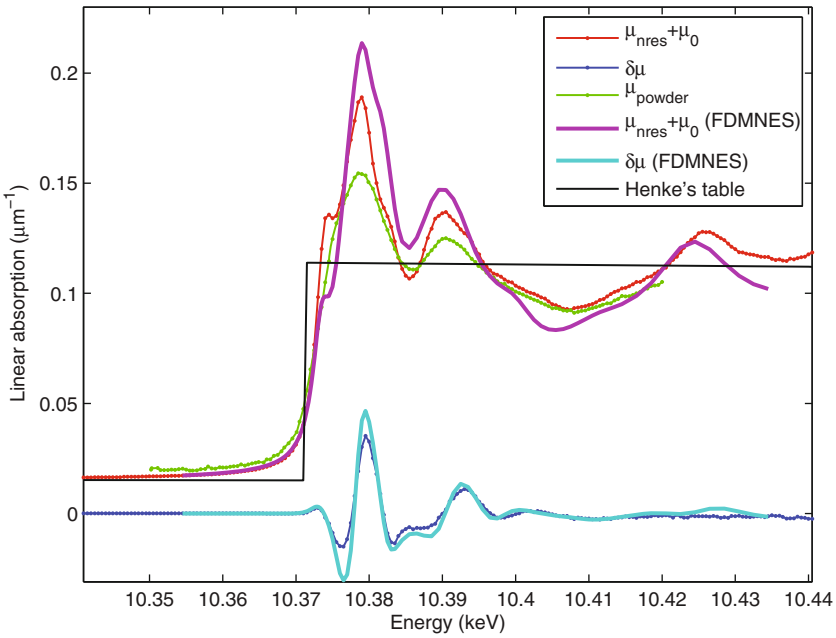

Fig. 7. Isotropic ($\mu_{nres}+\mu_0$) and anisotropic ($\delta\mu$) spectra of the linear absorption coefficient. The curves obtained by fitting the fluorescence data of Fig. 6 are compared to the powder absorption spectrum measured in transmission, and to calculations with the code FDMNES. For comparison, the values calculated from Henke's tables [39] are shown. There is no scaling factor, except for the powder absorption spectrum. The energy scale of the latter was also offset by 1 eV, which is attributed to the different calibrations of the two beamlines. The energy scale of the simulations were arbitrarily offset. The offset is not relevant for the calculations. The general shape of the experimental curves (fluorescence data) is in agreement with the FDMNES calculations: all features are present, only the amplitude of variations differs.

for the geometries of the RXS measurements agree globally well with the spectra recorded with the diffraction data (Fig. 6).

Interestingly, the isotropic spectrum measured by transmission of a powder is less contrasted than the same spectrum retrieved from the fluorescence measurements. The differences in the 'sharpness' and offset of the fluorescence and powder data are likely to be due to a combination of the difference in energy resolution between the two measurements (made at different beamlines), and the granular nature of the thin powder sample. This suggests that the isotropic spectrum retrieved from the fluorescence measurement are more reliable than the one directly measured on a powder. We used the latter one however to correct the RXS spectra, in order to be able to make a direct comparison with the ZnO data obtained in the same manner.

References

1. D.H. Templeton, L.K. Templeton, Acta Cryst. A **36**, 237 (1980)
2. V.E. Dmitrienko, Acta Cryst. A **39**, 29 (1983)
3. V.E. Dmitrienko, Acta Cryst. A **40**, 89 (1984)
4. D.H. Templeton, L.K. Templeton, Acta Cryst. A **41**, 133 (1985)
5. E.N. Ovchinnikova, V.E. Dmitrienko, Acta Cryst. A **56**, 2 (2000)
6. K.D. Finkelstein, Qun Shen, S. Shastri, Phys. Rev. Lett. **69**, 1612 (1992)

7. M. Fabrizio, M. Altarelli, M. Benfatto, Phys. Rev. Lett. **80**, 3400 (1998)
8. L. Paolasini, C. Vettier, F. de Bergevin, F. Yakhou, D. Mannix, A. Stunault, W. Neubeck, M. Altarelli, M. Fabrizio, P.A. Metcalf, J.M. Honig, Phys. Rev. Lett. **82**, 4719 (1999)
9. S. Di Matteo, Phys. Rev. B **70**, 165115 (2004)
10. S.B. Wilkins, S. Di Matteo, T.A.W. Beale, Y. Joly, C. Mazzoli, P.D. Hatton, P. Bencok, F. Yahkou, V.A.M. Brabers, Phys. Rev. B **79**, 201102(R) (2009)
11. V.E. Dmitrienko, E.N. Ovchinnikova, Acta Cryst. A **56**, 340 (2000)
12. V.E. Dmitrienko, E.N. Ovchinnikova, K. Ishida, JETP Letters **69**, 938 (1999)
13. J. Kokubun, M. Kanazava, K. Ishida, V.E. Dmitrienko, Phys. Rev. B **64**, 073203 (2001)
14. A. Kirfel, J. Grybos, V.E. Dmitrienko, Phys. Rev. B **66**, 165202 (2000)
15. S.P. Collins, D. Laundy, V.E. Dmitrienko, D. Mannix, P. Thompson, Phys. Rev. B **68**, 064110 (2003)
16. E.N. Ovchinnikova, V.E. Dmitrienko, K. Ishida, A. kirfel, S.P. Collins, A.P. Oreshko, D. Cabaret, R.V. Vedrinskii, V.L. Kraizman, A.A. Novakovich, E.V. Krivitskii, B.P. Tolochko. Nucl. Instr. Meth. Phys. Res. A **543**, 122 (2005)
17. E.N. Ovchinnikova, A.P. Oreshko, V.E. Dmitrienko, G. Beutier, S.P. Collins. J. Phys.: Condens. Matter **22**, 355404 (2010)
18. H. Schulz, K.H. Thiemann, Solid State Comm. **23**, 815 (1977)
19. H. Schulz, K.H. Thiemann, Solid State Comm. **32**, 783 (1979)
20. *International Tables for Crystallography*, volume A. (2005)
21. *International Tables for Crystallography*, volume D. (2010)
22. Note that our definition of x and y is different from that of [20] and [21] but consistent with [15]
23. G. Beutier, E. Ovchinnikova, S.P. Collins, V.E. Dmitrienko, J.E. Lorenzo, J.-L. Hodeau, A. Kirfel, Y. Joly, A.A. Antonenko, V.A. Sarkisyan, A. Bombardi. J. Phys.: Condens. Matter. **21**, 265402 (2009)
24. J. Goulon, N. Jaouen, A. Rogalev, F. Wilhelm, C. Goulon-Ginet, C. Brouder, Y. Joly, E.N. Ovchinnikova, V.E. Dmitrienko, J. Phys.: Condens. Matter. **19**, 156201 (2007)
25. S.W. Lovesey, E. Balcar, J. Phys.: Condens. Matter. **20**, 122201 (2008)
26. Y. Joly, Phys. Rev. B **63**, 125120 (2001), software available at `www.neel.cnrs.fr/fdmnes`
27. S.W. Lovesey, E. Balcar, K.S. Knight, J. Fernández Rodríguez, Physics Reports **411**, 233 (2005), This is a consequence of equation 120 for the rank K=3
28. A.M. Kolchinskaya, V.E. Dmitrienko, S.P. Collins, E.N. Ovchinnikova, A.P. Oreshko, Crystallography Reports **52**, 604 (2009)
29. A. Yoshiasa, K. Koto, F. Kanamaru, S. Emura, H. Horiuchi, Acta Cryst. B **43**, 434 (1987)
30. R.W. James, *The Optical Principles of the Diffaction of X-rays* (Ox Bow Press, Woodbridge, Connecticut, 1964)
31. I. Gorczyca, N.E. Christensen, E.L. Peltzer y Blancá, C.O. Rodriguez, Phys. Rev. B **51**, 11936 (1995), Table II and references therein
32. M. Schowalter, A. Rosenauer, J.T. Titantah, D. Lamoen, Acta Cryst. A **65**, 227 (2009)
33. X. Xiong, S.C. Moss, J. Appl. Phys. **85**, 2308 (1997)
34. B.A. Danilchenko, T. Paszkiewicz, S. Wolski, A. Jezowski, T. Plackowski, Appl. Phys. Lett. **89**, 061901 (2006), Table I and references therein
35. Y.-N. Xu, W.Y. Ching. Phys. Rev. B **48**, 4335 (1993), and references therein
36. C. Brouder, J. Phys.: Cond. Matter. **2**, 701 (1990)
37. P. Pfalzer, J.-P. Urbach, M. Klemm, S. Horn, L. denBoer Marten, I. Frenkel Anatoly, J.P. Kirkland, Phys. Rev. B **60**, 9335 (1999)
38. J.B. Kortright, A.C. Thompson, *X-ray data booklet* (Lawrence Berkeley National Laboratory, 2001), p. 1
39. B.L. Henke, E.M. Gullikson, J.C. Davis, *Atomic Data and Nuclear Data Tables* **54**, 181 (1993)
40. unpublished data